# Open-Chip Droplet Splitting in Electrowetting

*Nitish Sagar[†], Shubhi Bansal[†] and Prosenjit Sen**

[†]Equal contribution

Nitish Sagar, Shubhi Bansal and Prosenjit Sen
Centre for Nano Science and Engineering
Indian Institute of Science, Bangalore, India
E-mail: prosenjits@iisc.ac.in

Keywords: open-chip platform, electrowetting, splitting, compound droplet

**Abstract**

Electrowetting-on-dielectric (EWOD) has emerged as a powerful technique to perform on-chip droplet operations like transportation, dispensing, splitting, and mixing in sandwiched droplets. In contrast, open chip droplet manipulation using electrowetting enables micro-total-analysis systems with multiple sensor integration and re-routing capabilities. Droplet splitting has been the bottleneck in developing open-chip platforms. We present droplet splitting on an open chip platform using electrowetting-on-dielectric. We have developed an energy-based simulation model. It shows that splitting a sessile water droplet is impossible on an open-chip configuration because of the low pad contact angle requirement. Low contact angles cannot be achieved due to contact angle saturation in electrowetting. We experimentally show that splitting is possible if the droplet is engulfed in an oil shell (i.e., in compound droplets). We identify the planar electrode configurations and regime of electrowetting numbers for which splitting can be achieved. We observe that larger gaps and higher electrowetting numbers favour symmetrical splitting because the electrostatic force driving the actuation is significantly higher than the retarding interfacial forces. Conversely, asymmetrical splitting has been obtained when the actuation force is barely sufficient. We further demonstrate the splitting of surfactant-loaded single-phase sessile droplets and explain it using a preferential surface charging phenomenon.

## 1. Introduction

Digital microfluidics involves manipulating discrete droplets on patterned surfaces to develop lab-on-chip devices and micro total analysis systems. There are several different techniques like surface acoustic waves,[1][2][3] magnetic force,[4] thermo-capillary,[5] dielectrophoresis,[6] and electro-capillarity[7] to move the droplets on a chip. Electro-capillarity is one of the most favorable techniques to integrate, program, and control liquid movement using voltage-based actuation. Electro-capillarity refers to the change in the surface tension of an interface due to an applied electric field. Change in liquid-liquid interfacial tension for actuating liquids is known as continuous electrowetting. Whereas, in electrowetting-on-dielectric (EWOD), the droplets are actuated by applying an electric field across a dielectric.[8][9] Electrowetting on Dielectric (EWOD) is one of the most commonly used techniques for droplet manipulation. In digital microfluidics platforms,[10][11][12] EWOD has been used for numerous applications like mixing,[13] heating,[14] and sensing.[15] Conventionally, closed or sandwich droplet configuration[16] is used for transporting, splitting, merging, and dispensing droplets. The liquid is manipulated in the gap between two substrates in this configuration. Coplanar open-chip designs have also been used in the literature to move the droplets.[17][18] Here, the sessile droplets are manipulated on a single substrate in an open-chip configuration, and the top coverslip is not present.

Out of different droplet manipulations, splitting of the droplet is one of the most complicated tasks.[19][20] Laterally offset modulated SAW,[21] and integrated electrowetting devices [22] have been used to split droplets. Droplet splitting is useful for on-chip sample separation and micro-extraction.[23] In conventional EWOD, the splitting of droplets is performed using three consecutive electrodes on a sandwich device. The actuation causes the droplet to spread on three or more consecutive electrode patterns. Surface energy minimization-based approach has been used to develop the required criterion for droplet splitting in sandwich configuration[24]. Several efforts have been made for precise droplet dispensing and cutting based on different electrode geometries.[25][26] The coplanar electrode configuration has been used inside microchannel for droplet manipulation.[27] However, on the planar open-chip, the droplet contact line doesn't satisfy the condition for forming negative curvature in the ground electrode region, which is an essential criterion for droplet splitting.[19] Splitting sessile droplets in an open-chip configuration is an existing challenge that has hindered the development of open-chip microfluidic devices.[17]

Recently, splitting of droplet on open microfluidic platform has been proposed for the first time using dielectrowetting.[28] In dielectrowetting, super spreading beyond contact angle saturation has been demonstrated.[29] 23° contact angle was reported at 300 V by using interdigitated electrode patterns. Dielectrowetting has been shown to cause droplet splitting for both conductive (aqueous) and non-conductive (propylene carbonate) solutions. But the splitting of droplet is shown only with propylene carbonate droplets. To date, splitting of droplet on open EWOD platform has not been achieved to the best of the author's knowledge.

This work presents energy-based reasoning to explain why splitting of DI water on an open-chip configuration has not been possible. A possible solution is presented to split compound droplets on an open-chip device. Symmetric droplet splitting and asymmetric droplet creation have been demonstrated. The technique is thoroughly studied to understand the splitting behaviour and characterize the role of different parameters. Splitting of surfactant added droplet on open-chip EWOD is also presented. The role of preferential dielectric charging, in this case, has been explained.

Compared to the conventional EWOD, an open platform allows more accessibility for integrating multiple functionalities and operations. Further, compound droplet (of sample core and oil shell) splitting facilitates easier handling of biological and colloidal samples preventing their contamination, evaporation, and surface pinning.

## 2. Experimental methods

### 2.1. Device design and fabrication

The devices were made on Borofloat glass wafers. ITO (Indium Tin Oxide, 150 nm) was sputtered to make the transparent actuation electrodes to enable bottom view imaging of the droplet. An optical lithography technique was used to pattern the electrodes. Two electrodes were patterned each with a size of 3.5 mm x 3.5 mm for the symmetrical electrode design. The electrodes were separated by a gap ranging from 0.5 mm to 1.5 mm. Asymmetrical electrode design consisted of a 3.5 mm x 3.5 mm large electrode and a 1 mm X 1 mm small electrode. The inter-electrode gap of 1040 microns was used. SU8 2005 (5 ± 0.3 μm) was used as the dielectric layer on the metal. Teflon® (DuPont, AF-2400) was spin-coated at 5000 rpm for 40 s to form the topmost hydrophobic layer of 170 ± 30 nm thickness. Silicone oil (1 cSt) was used as the shell for the compound droplet.

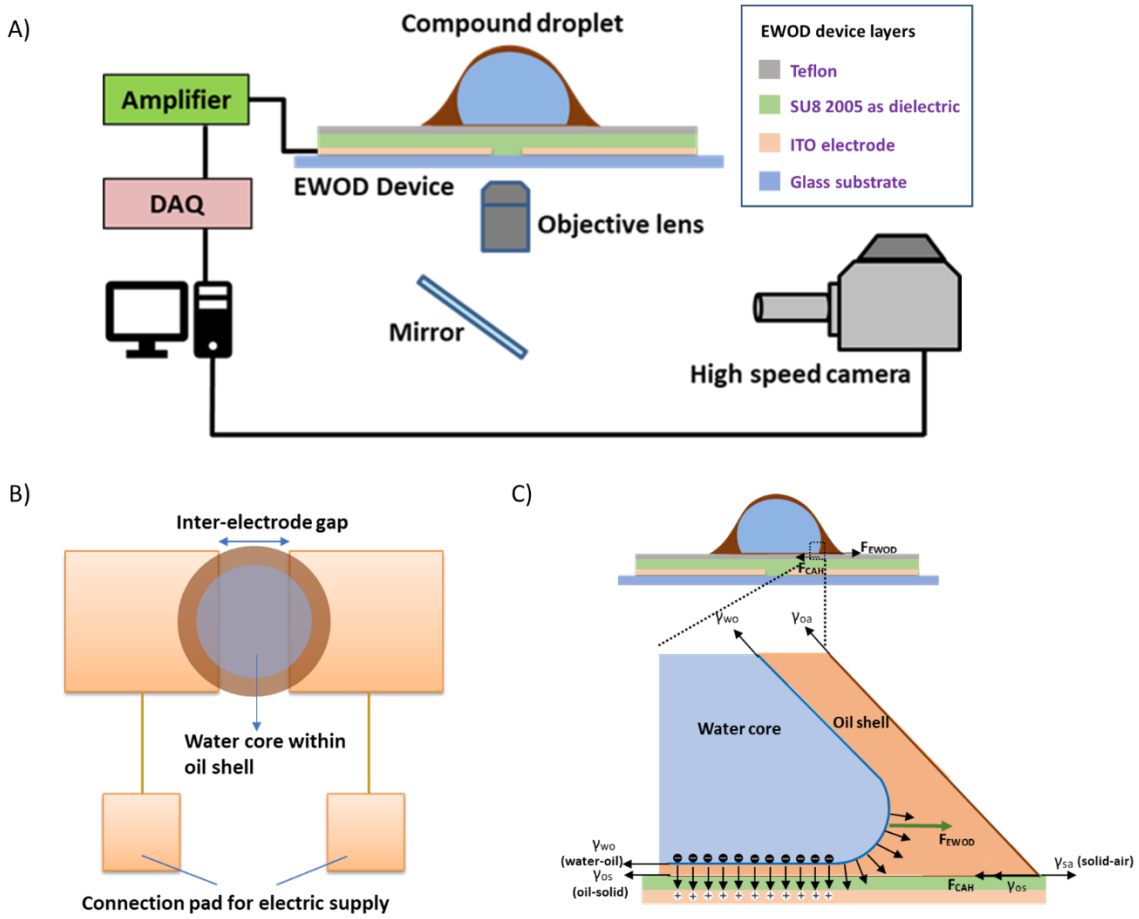


Figure 1. A) Schematic of the experimental setup for bottom imaging. EWOD device layers are shown in the box. B) Figure illustrating placement of the compound drop on the device within the inter-electrode gap in bottom view imaging. C) Schematic representation of forces acting on droplet in electrowetting. Inset figure shows the magnified image of water-oil interface.

### 2.2. Experimental Setup

The experiments were performed by varying the actuation voltage from 200 V to 450 V DC pulse in the step of 50 V. A National Instruments DAQ card (NI-DAQ 6363) was used to apply the DC pulse voltage. The generated signal was amplified using a high voltage amplifier (Trek 2205) by a gain of 50. The videos were recorded using a high-speed camera (Photron SA4 Fastcam) at a frame rate of 250-5000 fps. The bottom view imaging was done to observe the droplet splitting dynamics. The schematic of the experimental setup is shown in Figure 1A. The droplet was dispensed using a micro-pipette. It was placed in the gap between electrodes such that the interface of the droplet touches both the electrodes. DC pulse of 1s pulse width was applied across the electrodes (Figure 1B). The experimental setup temperature is not controlled. However, the lab is air-conditioned, and the temperature is maintained between 23°C to 25°C. In the absence of electrowetting, different interfacial surface energies determine the equilibrium droplet shape. The different interfacial energies are: (i) $\gamma_{wo}$ is the surface tension of the water-

oil interface, (ii) $\gamma_{os}$ is the surface tension of the oil-solid interface, (iii) $\gamma_{sa}$ is the surface tension of the solid-air interface, and (iv) $\gamma_{oa}$ is the surface tension of the oil-air interface. The contact angle is defined by Θ that is the resultant of force balance between all the interfacial forces. During actuation, the solid-liquid interfacial tension is reduced proportional to the charge density.[30] The electrowetting actuation force ($F_{EWOD}$) acts on the droplet interface on top of the actuation electrode that is equals to the negative gradient of the interfacial energy (Figure 1C). The split electrode configuration tries to pull the droplet to opposite sides. Contact angle hysteresis restricts the motion acts on the oil-solid interface. In the case of a compound sessile droplet, contact angle hysteresis on inner core droplet reduces due to oil shell around it.

### 2.3. Statistical Analysis

We used Photron FASTCAM Viewer (PFV4) and ImageJ software to analyze the high-speed videos. Dimensions in images were calculated using a calibration factor (μm / pixel) that was estimated using known dimensions on the chip. Experiments were repeated five times, and the results plot mean and standard deviation. For all the statistical analysis, we have used the plotting software Origin.

## 3. Results and discussion

### 3.1. Challenges in open chip droplet splitting

Splitting a 1 μL water droplet was not possible in an open chip configuration. Upon actuation with a 200 V pulse, the droplet spreads on the active electrode pads without splitting (see Supplementary Information Figure 1S). At higher actuation voltages, the droplet leaves the gap and moves towards one of the electrodes. Similar behavior was observed for various inter-electrode gaps and actuation voltages. We performed surface evolver simulations to explain this observation. Using the Surface Evolver software, we studied minimal energy shapes of half-droplet (imposing central symmetry). The surface energy constraints were imposed on the contact line by specifying the contact angles (Figure 2). The inter-electrode region retains its original contact angle of 120°. At the same time, the contact angle on top of the electrode pad (pad contact angle) is reduced due to electrowetting. In the simulations, the pad contact angle was varied between 50° and 110°. The surface tension of the droplet is taken is 72 mN/m. The inter-electrode gap was fixed as 1000 μm for simulation. The droplet radius is varied from 0.7 mm to 1.6 mm.

Another geometrical constraint (boundary condition) used in the simulation is neck width. Neck width is the width of the liquid bridge formed in the inter-electrode region. The objective of the simulation is to get the minimum energy droplet shape for each pad contact angle. However, near the minimal energy configuration (droplet shape), the energy gradient becomes very small. The simulation often fails to converge to a minimal energy droplet shape. To overcome this problem, we introduce an additional shape constraint (boundary condition) in the form of the neck width. For a given pad contact angle, simulations are run to evaluate the surface energy for different neck widths. The equilibrium morphology was determined by considering how the surface energy drives the change of droplet shape (neck width).

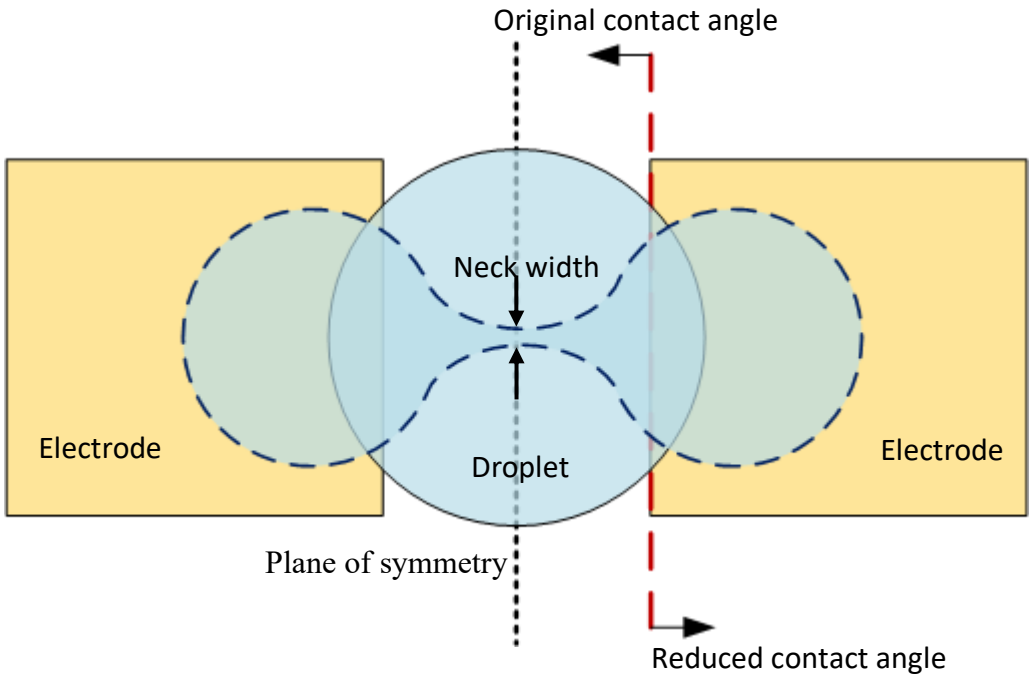


Figure 2. Schematic representation of droplet and electrode configuration solved using Surface Evolver.

Figure 3A shows the evolved half-droplet morphology for different neck width constraints when the pad contact angle is 80°. The inter-electrode gap to droplet radius (G/R) value is 1.43. Subfigure a-d shows drop shape for different neck width constraints. Neck width constraint reduces from a to d. Figure 3B plots the surface energy as a function of neck width for different pad contact angles. For pad contact angles greater than 60°, as the droplet neck width reduces, surface energy first increases and then suddenly dips to a lower value. This dip is due to an unstable neck at smaller neck width constraints. However, this does not imply splitting as the initial energy increase leads to an energy barrier.

The droplet will spontaneously split only when there is no energy barrier, and the surface energy continuously reduces with a reduction in neck width. This case is observed when the pad contact angle is further reduced to 60°. Here energy at full neck width is higher than at smaller neck widths. Figure 3C shows the neck width at which the surface energy is maximum. It has been plotted for different pad contact angles and G/R ratios. Below a critical pad contact angle, energy is maximum for the initial configuration (i.e., without electrowetting). This pad contact angle is the onset point of spontaneous droplet splitting.

We have simulated different droplet sizes. As the droplet size is increased, spontaneous splitting occurs at lower pad contact angles. Figure 3D shows the critical pad contact angle required for drop splitting for different G/R values. The droplet splits at a higher contact angle for larger G/R ratios. However, the critical angles for splitting lie below 60°. Figure 3E plots the experimental measurements of contact angle change with applied voltage. The contact angle is observed to saturate at 78°. Contact angle saturation is a well-studied phenomenon.[31] Once the saturation angle is attained, the contact angle does not reduce further by increasing the voltage. Thus, it is impossible to split DI water on an open-chip EWOD configuration. We have also considered simulations with lower surface tension droplets (see Supplementary Information Figure 2S). We observe similar critical contact angles (< 60°) for splitting. The results indicate that only lowering surface tension will not help in splitting droplets in an open chip configuration.

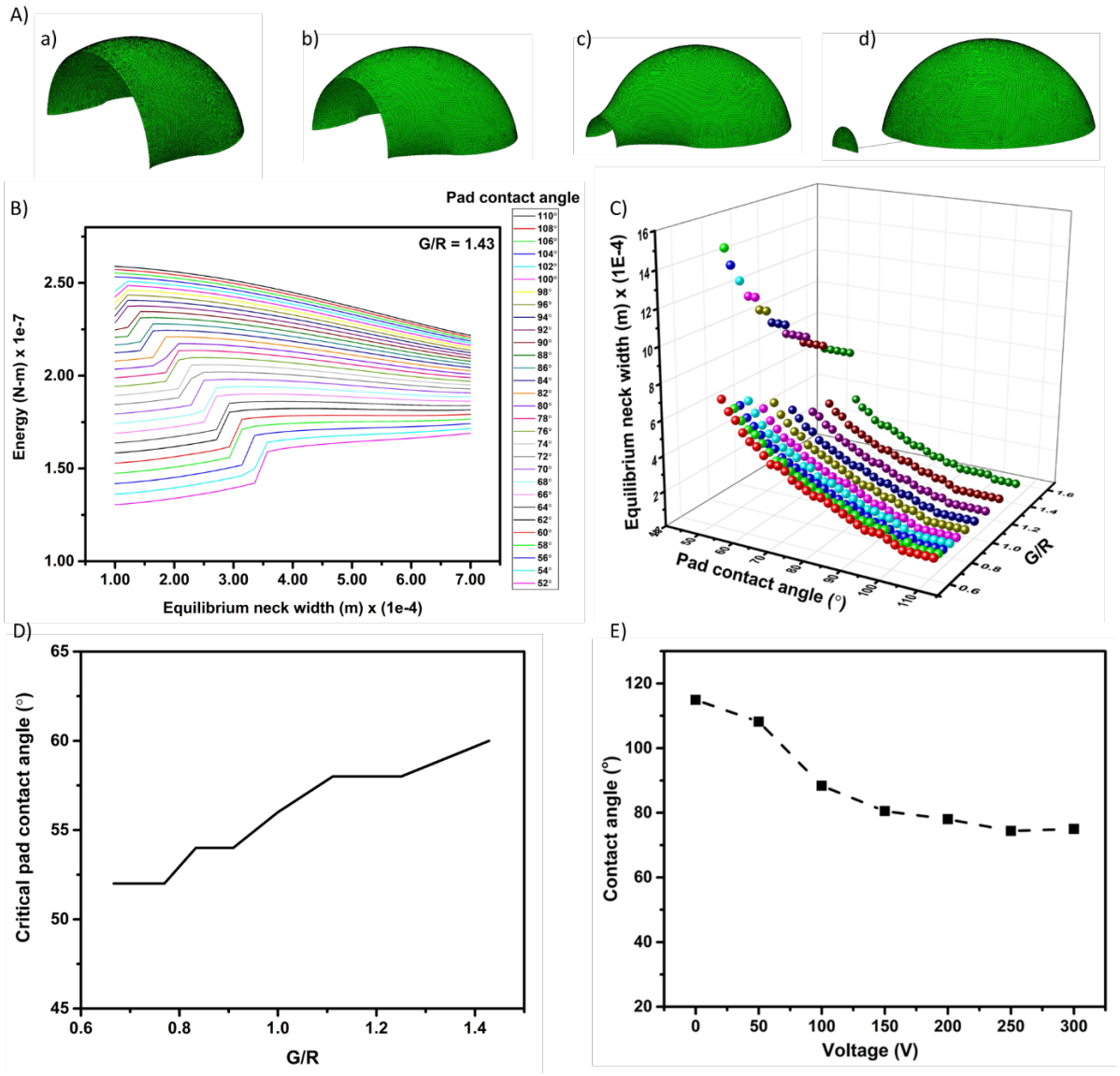


Figure 3. A) Simulation profiles of the droplet morphology for different neck width constraints. B) Variation of droplet surface energy (G/R =1.43) with neck width constraints for different pad contact angles. C) 3D scatter plot showing the equilibrium neck width for maximum droplet energy with pad contact angles for different G/R ratios. D) The critical pad contact angle for splitting for different G/R ratio. E) Young-Lipmann plot of DI water showing contact angle saturation.

### 3.2. Compound droplet splitting

Splitting droplets in an open chip configuration has been challenging primarily due to difficulty in forming necks (bridges) in an open-chip configuration. The 3-dimensional necks formed in an open-chip configuration have a large negative curvature, which drives the liquid towards the neck and prevents its thinning. Additionally, contact angle hysteresis force acting on the contact

line hinders the necking process. Liquid bridges on a substrate are inherently stable against splitting and do not break by themselves.[32] This was confirmed in our experiments with DI water. Both limitations can be addressed by using a compound droplet configuration, where an oil droplet covers the water droplet. The splitting of compound droplets was achieved in this work in an open-chip configuration using DC EWOD. Compound droplets were formed with two immiscible liquids – DI water as the core droplet and silicone oil as the shell droplet.[33] Silicone oil (1 cSt) was used as the compound droplet's shell. The compound droplet is formed by the pipetting technique. DI water is initially placed between the inter-electrode gap. Then silicone oil is pipetted on the top of DI water to form the shell. Since the surface tension of silicone oil is much lower than that of water, energy minimization governs the formation of an oil film around water.[34][35]

The droplet is placed manually by pipetting DI water and silicone oil in the inter-electrode gap. There are some errors in initial placement as the droplet is positioned visually. However, the system is self-centring (see Supplementary Information Figure 3S). Once the voltage is applied, the droplet automatically self-centres. Hence, we do not expect a large effect due to the initial positioning. Two different cores to shell volume ratios were used in this study 5:1 and 1:1. The compound droplet was placed between the electrodes with its core overlapping both the electrodes, as shown in Figure 4. Depending on the operating parameters, we observed both symmetrical as well as asymmetrical splitting. In symmetrical splitting, the split droplets were approximately the same size. The split droplets had significantly different volumes in asymmetrical splitting.

A 1s DC pulse actuation was used to split the droplet. The dynamics of the symmetrical splitting process are shown in Figure 4A. When the actuation was turned "on", the interface on both the electrodes spread. This causes the formation of a neck in the region between the electrodes. The neck breaks, and the droplet splits. Since the surface tension of silicone oil is much lower than that of water, an oil film surrounds the water drop[36]. The oil film between the substrate and the droplet lowers hysteresis, which enables easy interface motion. Further, the core drop bridge in the electrode gap does not contact the substrate even when actuated. This helps in the formation and breakage of the cylindrical neck by the Rayleigh-Plateau instability.

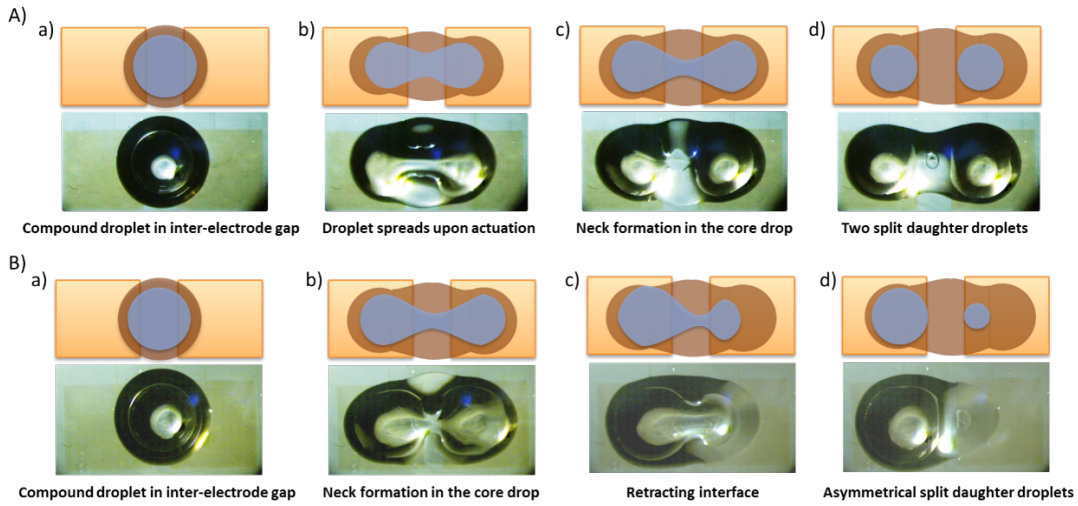


Figure 4. Schematic representation and snapshots of different stages of compound droplet splitting. A) Symmetrical splitting of 5 µl DI core in 1 µl oil shell on open EWOD device actuated by 300 V DC pulse. The inter-electrode gap is 1500 µm. B) Asymmetrical splitting of 5 µl DI core in 1 µl oil shell on open EWOD device actuated by 400 V DC pulse. The inter-electrode gap is 750 µm.

Asymmetrical splitting was observed at low voltage or in devices with low inter-electrode gaps. Figure 4B shows the snapshots of the progression of splitting stages for an inter-electrode gap of 750 µm at 400 V. Like symmetrical splitting, the neck formation was observed. However, one of the interfaces starts retracting after neck formation, as shown in Figure 4B. Finally, the neck breaks, creating one large droplet and one small daughter droplet. The effect of actuation voltage, electrode gap, and core-shell volume ratio on the asymmetric/symmetric splitting regime was studied. The left-right symmetry breaks in the case of asymmetrical splitting. The symmetry breaks only after the initiation of the splitting process as seen in Figure 4B. Symmetrical splitting is observed at higher actuation voltages. We believe that the asymmetrical splitting at lower voltages is due to the low actuation force available for splitting. At low actuation forces, flow velocities are small, and existing asymmetries in the system (e.g., inherent surface asymmetries) can drive the flow to be asymmetric.

Figure 5 shows the splitting regime as a function of the Electrowetting number ($Ew$) and the normalized electrode gap. Electrowetting number is defined as $Ew = cV^2/2\gamma_{ow}$, where $c$ is the capacitance per unit area, $V$ is the applied voltage, and $\gamma_{ow}$ is the surface tension of the oil-water interface. The electrode gap is normalized by the size of the core droplet calculated as $\sqrt[3]{\Omega}$ (where Ω is the volume of the core drop). The experiments were performed more than five times for each operating parameters to deduce this splitting regime. No splitting was obtained for electrowetting numbers below 3.16 for the core to shell volume ratio of 5:1 (Figure 4a). The

droplet spreads on electrodes without any neck formation. This is because the actuation force is not sufficient to form necking. Similarly, at a lower inter-electrode gap of 500 µm, no splitting was observed. Smaller gaps require necks with a smaller radius of curvature for splitting. Actuation forces due to EWOD are insufficient to overcome the considerable negative Laplace pressure in such necks with smaller radius of curvature.

Above these thresholds of $Ew$ and normalized gap ($G/\sqrt[3]{\Omega}$), asymmetric splitting was observed at lower electrowetting numbers and smaller $G/\sqrt[3]{\Omega}$ values (see Figure 5a). In this regime, the actuation force is barely sufficient to cause splitting. Hence, a slight variation in the Laplace pressure can drive the liquid flow from one side to the other. Surface heterogeneities lead to a variation of the local forces and hence Laplace pressure. Symmetric splitting was observed at higher electrowetting numbers and larger $G/\sqrt[3]{\Omega}$ values. At the boundary of these regimes, we observe both symmetrical and asymmetrical splitting. Blue triangles show these data points in Figure 5a. The outcome is not controllable. We believe that the mixed outcome results from the random nature of surface heterogeneity. Its effect changes with each experiment due to the inaccuracies in the initial droplet placement.

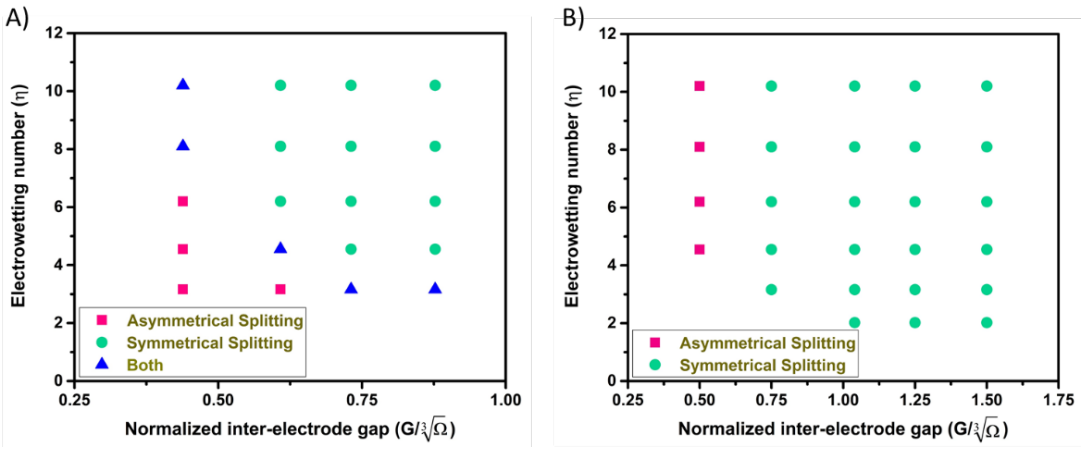


Figure 5. A) Splitting regimes as a function of electrowetting number (η) and interelectrode gap for core-shell ratio (5:1). B) core-shell ratio (1:1).

We then reduced the core-shell volume ratio to 1:1, implying an equal water and oil volume of 1µL. Figure 5b shows the splitting regime at different gaps. Asymmetrical splitting is observed at the normalized inter-electrode gap of 0.5. Symmetrical splitting for 1:1 core to shell volume is achieved at a larger inter-electrode gap. We do not observe boundary points where both symmetrical and asymmetrical splitting co-exist. The critical electrowetting number for splitting is also reduced to 2.02. Our observation implies that by increasing the shell (oil)

volume, droplet splitting is achievable at a lower electrowetting number. This can be attributed to the reduced effect of the oil-air surface tension in the overall phenomena at larger oil volumes. The simulation result in the previous section shows that the pad contact angle required to split droplet increases (thus, the voltage required decreases) with an increase in the G/R (gap/drop-size) ratio. The experimental result also suggests that as the G/R ratio increases, symmetrical splitting is observed at lower voltages. Thus, our energy-based numerical study supports the regime plot obtained by experiments in Figure 5. As flow asymmetries drive the asymmetrical splitting, our simulations cannot predict the asymmetrical vs. symmetrical regimes.

The time required for splitting has been measured for 5:1 core to shell volume ratio as shown in Figure 6A. At larger normalized inter-electrode gap, mean split time was found to be within 30 ms. Deviation in split time is smaller at larger gaps. This depicts the symmetrical splitting of droplet which breaks instantaneously. At lower normalized gaps than 0.6, we have observed higher mean split time at low voltage due to asymmetrical splitting. Asymmetrical splitting involving liquid drainage and interface motion is a significantly slower process.[37][38] As the voltage was increased, mean split time reduces as symmetrical splitting regime is reinstated. This shows that asymmetrical splitting is dominant at low voltage while symmetrical splitting can be seen at higher voltage. We found that non-uniform retraction velocity of the interface in case of asymmetrical splitting was the reason for the large variation in split time.

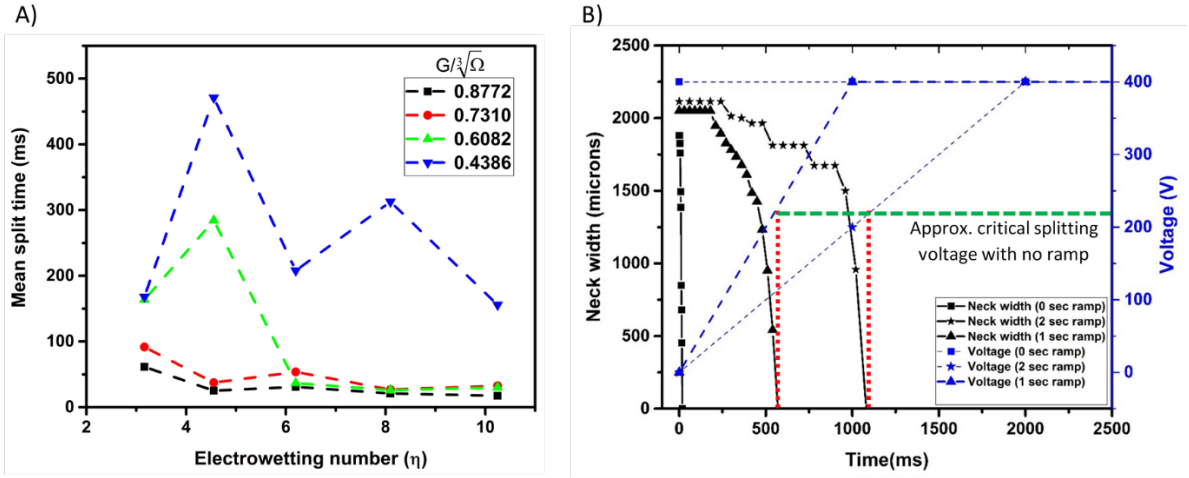


Figure 6. A) Variation of mean split time for 5:1 core to shell volume ratio droplet with electrowetting number (η) for different normalized inter-electrode gaps ($G/\sqrt[3]{\Omega}$). B) Plot demonstrating transition of neck width of droplet during slow ramp of applied voltage.

We have performed experiments of compound droplet splitting with slow ramp of the applied voltage (Figure 6B). In this experiment, we have taken 1 µL of DI water as core droplet and 1

µL of silicone oil as the surrounding shell. The inter-electrode gap is taken as 1500 µm. The applied voltage is slowly ramped from 0V to 400V with different ramp times (0s, 1s and 2s) for 5s pulse width. We have measured the variation in the droplet neck width with time for different ramp time experiments. As shown in the above figure, for 0s ramp time, we observe sudden decrease in the neck width within 20 ms time. This sudden decrease in the neck width leads to splitting of the droplet. When the voltage is slowly ramped for 1 s, we observed constant neck width for initial duration of 200 ms. The neck width slowly reduces after that for some time, and suddenly the there is a large reduction in neck width after 500ms. Similarly, for 2 sec ramp time, neck width reduction is further slowed down and we observe splitting after 1sec. This experiment proves that splitting of compound droplet is not an inertial phenomenon, rather it is viscous dominated.

### 3.3. Droplet creation for compound droplets

The asymmetric electrode pattern was explored for controlled asymmetric splitting. Controlled asymmetrical splitting is required in droplet generation operation. A 1040 µm gap separated the pads. The compound droplet was placed between the reservoir and the electrode, as shown in Figure 7A. Upon actuation, the interface on the smaller electrode spread to cover the maximum area (Figure 7B). Subsequently, the droplet is pulled back towards the bigger electrode because its greater contact line length provides a larger pulling force. This pulling causes necking and formation of a droplet on the smaller electrode.

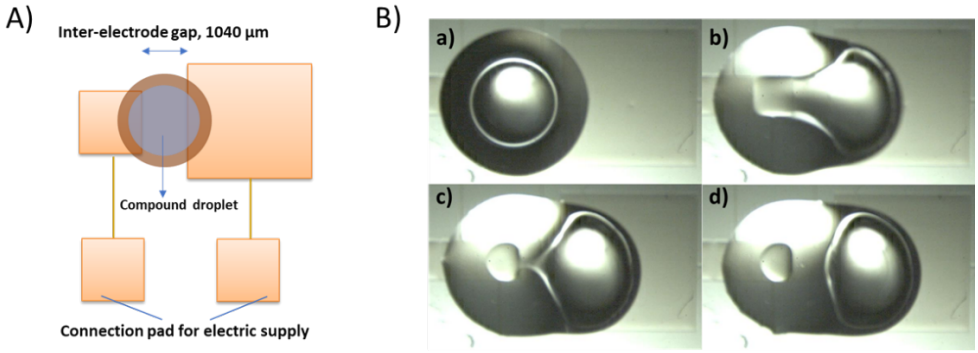


Figure 7. A) Schematic representation of electrode configuration for an asymmetrical design. B) The experimental images showing splitting of a compound droplet having 1 µl core and 1 µl shell on open EWOD space by 350 V DC actuation pulse: a) initial position b) spreading interface c) neck formation d) daughter droplets formed by pinch-off.

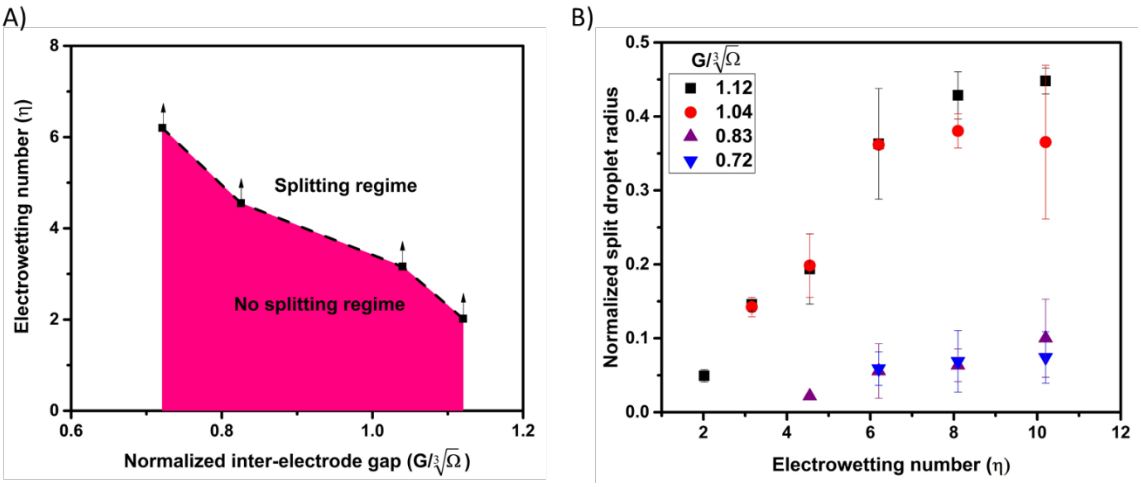


Figure 8. A) The graph marks the boundaries of minimum threshold electrowetting number needed to obtain splitting of compound droplet for different $G/\sqrt[3]{\Omega}$ in the given EWOD configuration. B) The normalized split droplet radius variation with electrowetting number for different $G/\sqrt[3]{\Omega}$ ratio.

Compound droplet generation was tried for different core volumes (0.8 µl to 3 µl). Critical electrowetting number for splitting was determined as shown in Figure 8a. Below this voltage, the interfaces spread on the two actuation electrodes, but they did not split. The interface retraced back to its initial position. The threshold electrowetting number needed to obtain droplet splitting was found to increase with the increase in core volume (or decrease in the normalized gap $G/\sqrt[3]{\Omega}$ values). The effect of electrowetting number on the size of the generated drop is shown in Figure 8b. For the same core volume, when the applied voltage was increased, the radius of split drops increased. This can be attributed to increased droplet spreading at higher voltages on both the electrodes and faster retraction because of larger pulling force. Also, we observed that split daughter droplet volume is more for larger $G/\sqrt[3]{\Omega}$ ratio. As we have seen from the simulation result larger $G/\sqrt[3]{\Omega}$ ratio assists in splitting (instantaneous breaking of neck without retracting), it explains larger daughter droplet.

### 3.4. Surfactant-added droplet splitting

Splitting of surfactant-added droplets was also attempted. Tween20 was used as a surfactant at a 3% concentration. The CMC value of Tween 20 in DI water is 0.06%.[39] The surface tension of the solution was measured to be 35 mN/m using a Du Nouy tensiometer (see Supplementary Information Figure 4S). One µL droplets were dispensed in the inter-electrode gap. The droplet expands upon actuation due to electrowetting force. However, necking is not observed at the initial expansion phase. Subsequently, the droplet interface on one electrode starts retracting, and most of the liquid moves over to one of the electrodes. In the final stages of interface motion,

the smaller droplet becomes pinned to the electrode. This leads to necking, and finally, a daughter droplet pinched off at the edge, as shown in Figure 9A.

This experimental observation is contrary to our simulation results which show that the pad contact angles required for splitting do not change with a reduction in liquid surface tension (see Supplementary Information Figure 2S). The splitting of surfactant-added droplets is achieved at a much higher voltage. Further, the retraction of the interface is always observed on the positive pad. This indicates the trapping of charges in the dielectric. It also shows that a specific charge (negative in this case) will charge the dielectric preferentially. Hence, the electrowetting force on the interface above the positive pad is reduced, leading to the interface's retraction. As the droplet size reduces on the positive pad, the residual charge density on the smaller droplet increases. This causes the smaller drop to get pinned on the positive pad and subsequently drives the droplet necking and finally causes droplet pinch-off.

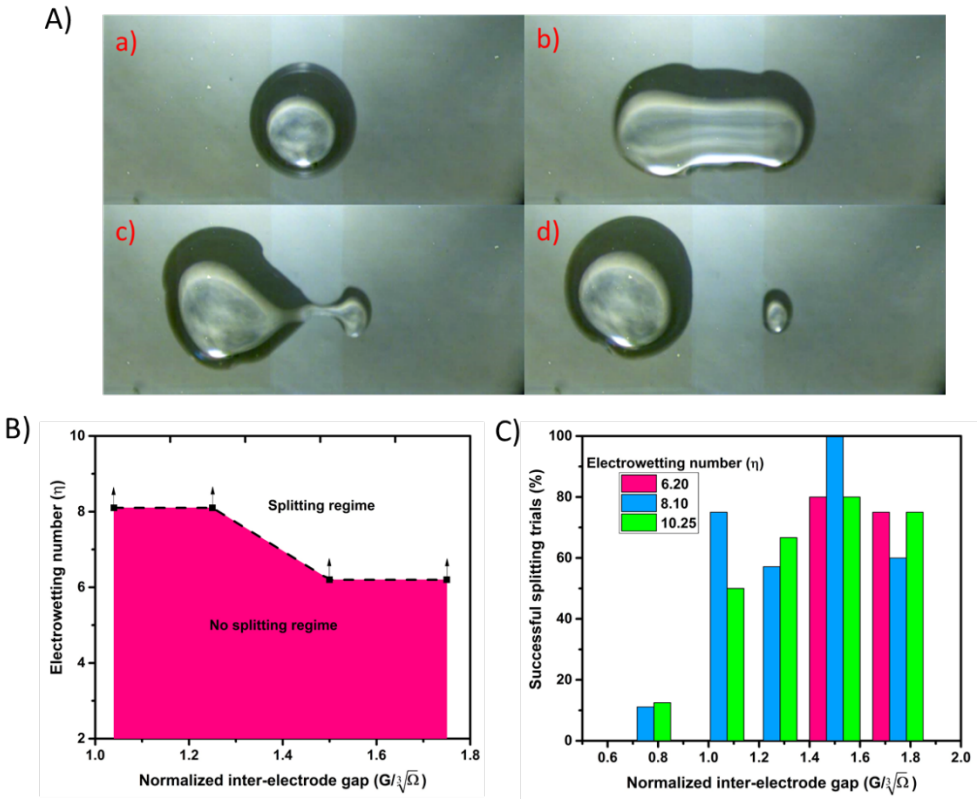


Figure 9. Asymmetrical splitting of Tween20 solution (3% volume fraction). The inter-electrode gap is 1500 μm. DC pulse of amplitude 350 V was applied across the pad. a) Before actuation b) Interface expands on the actuated pad c) Right side interface starts retracting leads to neck formation d) Split daughter droplet.

We determined a splitting regime where splitting can be achieved for different electrode gap and threshold voltage conditions. No splitting was observed below the 1.04 normalized gap, as shown in Figure 9B. For gaps equal to or larger than 1.04, we found a threshold voltage beyond which splitting was observed. Since this type of splitting depends on the dielectric charging effect, we repeated the experiments for each inter-electrode gap and voltage. Figure 9C shows the percentage of successful splitting for different experimental conditions. It can be inferred that the chance of splitting at gaps lower than 1.02 μm is less than 20%. As the inter-electrode gap increases, the probability of splitting reaches between 50% to 100%.

## 4. Conclusion

To date, the splitting of droplets has been limited to closed chip electrowetting configuration. The droplet splitting has been shown to be constrained by the gap between the top and the bottom plate, stating that lower gap between top and bottom plate favours splitting of the droplet. In this work, we achieve droplet splitting on an open-chip electrowetting-on-dielectric (EWOD) based microfluidic platform both experimentally and by simulation, for the first time to the best of the author's knowledge. We have also presented an energy-based analysis of open-chip droplet splitting. We have used compound droplet for open-chip droplet splitting. Different splitting regime have been obtained by varying electrowetting number and inter-electrode gap. We have been able to achieve symmetrical and asymmetrical splitting of droplets by varying electrowetting number and G/R ratio of the droplet. We have also shown splitting of surfactant-added droplet assisted by preferential charging of dielectric. The splitting of compound droplets will play a significant role in droplet manipulation on open lab-on-chip platforms for both aqueous and biological solutions. This will embark the pathway to establish a plethora of new opportunities like micro-total analysis systems with on-chip reagent splitting along with multiple sensor integration and re-routing capabilities.

## Supporting Information

Supporting Information is available from the Wiley Online Library or from the author.

**Acknowledgments**

The fabrication of the devices was done at the National Nanofabrication Facility supported by the Department of Science and Technology and the Ministry of Electronics and Information Technology.

Received: ((will be filled in by the editorial staff))
Revised: ((will be filled in by the editorial staff))
Published online: ((will be filled in by the editorial staff))

References

[1] A. Renaudin, P. Tabourier, J. C. Camart, C. Druon, *J. Appl. Phys.* **2006**, *100*, 1.

[2] D. Beyssen, L. Le Brizoual, O. Elmazria, P. Alnot, *Sensors Actuators, B Chem.* **2006**, *118*, 380.

[3] A. L. Zhang, Z. Q. Wu, X. H. Xia, *Talanta* **2011**, *84*, 293.

[4] Y. Zhang, N. T. Nguyen, *Lab Chip* **2017**, *17*, 994.

[5] J. Z. Chen, S. M. Troian, A. A. Darhuber, S. Wagner, *J. Appl. Phys.* **2005**, *97*.

[6] T. B. Jones, M. Gunji, M. Washizu, M. J. Feldman, *J. Appl. Phys.* **2001**, *89*, 1441.

[7] J. Lee, H. Moon, J. Fowler, T. Schoellhammer, C. J. Kim, *Sensors Actuators, A Phys.* **2002**, *95*, 259.

[8] F. Mugele, J. C. Baret, *J. Phys. Condens. Matter* **2005**, *17*.

[9] C. Quilliet, B. Berge, *Curr. Opin. Colloid Interface Sci.* **2001**, *6*, 34.

[10] W. C. Nelson, C.-J. Kim, *J. Adhes. Sci. Technol.* **2012**, *26*, 1747.

[11] F. Mugele, M. Duits, D. Van Den Ende, *Adv. Colloid Interface Sci.* **2010**, *161*, 115.

[12] M. G. Pollack, R. B. Fair, A. D. Shenderov, *Appl. Phys. Lett.* **2000**, *77*, 1725.

[13] S. Bansal, P. Sen, *Sensors Actuators, B Chem.* **2016**, *232*, 318.

[14] K. N. Nampoothiri, M. S. Seshasayee, V. Srinivasan, M. S. Bobji, P. Sen, *Sensors Actuators, B Chem.* **2018**, *273*, 862.

[15] S. Bansal, P. Sen, *J. Colloid Interface Sci.* **2020**, *568*, 8.

[16] M. G. Pollack, A. D. Shenderov, R. B. Fair, *Lab Chip* **2002**, *2*, 96.

[17] U. C. Yi, C. J. Kim, *J. Micromechanics Microengineering* **2006**, *16*, 2053.

[18] C. G. Cooney, C. Y. Chen, M. R. Emerling, A. Nadim, J. D. Sterling, *Microfluid.*

*Nanofluidics* **2006**, *2*, 435.

[19] S. K. Cho, H. Moon, C. Kim, **2003**, *12*, 70.

[20] A. Banerjee, Y. Liu, J. Heikenfeld, I. Papautsky, *Lab Chip* **2012**, *12*, 5138.

[21] S. Collignon, J. Friend, L. Yeo, *Lab Chip* **2015**, *15*, 1942.

[22] Y. Li, Y. Q. Fu, S. D. Brodie, M. Alghane, A. J. Walton, *2011 16th Int. Solid-State Sensors, Actuators Microsystems Conf. TRANSDUCERS'11* **2011**, 2936.

[23] P. A. L. Wijethunga, Y. S. Nanayakkara, P. Kunchala, D. W. Armstrong, H. Moon, *Anal. Chem.* **2011**, *83*, 1658.

[24] J. Berthier, O. Raccurt, P. Clementz, D. Jary, P. Claustre, C. Peponnet, Y. Fouillet, *2005 NSTI Nanotechnol. Conf. Trade Show - NSTI Nanotech 2005 Tech. Proc.* **2005**, *1*, 664.

[25] N. Y. J. B. Nikapitiya, M. M. Nahar, H. Moon, *Micro Nano Syst. Lett.* **2017**, *5*, 24.

[26] N. Y. J. B. Nikapitiya, S. M. You, H. Moon, *Proc. IEEE Int. Conf. Micro Electro Mech. Syst.* **2014**, 955.

[27] R. De Ruiter, A. M. Pit, V. M. De Oliveira, M. H. G. Duits, D. Van Den Ende, F. Mugele, *Lab Chip* **2014**, *14*, 883.

[28] H. Geng, J. Feng, L. M. Stabryla, S. K. Cho, *Lab Chip* **2017**, *17*, 1060.

[29] G. McHale, C. V. Brown, M. I. Newton, G. G. Wells, N. Sampara, *Phys. Rev. Lett.* **2011**, *107*, 1.

[30] W. C. Nelson, C. C. J. Kim, 37.

[31] A. Quinn, R. Sedev, J. Ralston, *J. Phys. Chem. B* **2005**, *109*, 6268.

[32] H. Gau, S. Herminghaus, P. Lenz, R. Lipowsky, *Science (80-. ).* **1999**, *283*, 46.

[33] M. J. Neeson, R. F. Tabor, F. Grieser, R. R. Dagastine, D. Y. C. Chan, *Soft Matter* **2012**, *8*, 11042.

[34] S. Bansal, P. Sen, *Langmuir* **2017**, *33*, 11047.

[35] S. Bansal, P. Sen, *J. Colloid Interface Sci.* **2018**, *530*, 223.

[36] S. Bansal, P. Sen, *Langmuir* **2017**, *33*, 11047.

[37] M. A. Bruning, M. Costalonga, S. Karpitschka, J. H. Snoeijer, *Phys. Rev. Fluids* **2018**, *7*, 1.

[38] S. Karpitschka, H. Riegler, *J. Fluid Mech.* **2014**, *743*, 1.

[39] A. Bąk, W. Podgórska, *Colloids Surfaces A Physicochem. Eng. Asp.* **2016**, *504*, 414.